Article

SOURCE DATA | TRANSPARENT PROCESS

EMBO reports

The tumor suppressor Brat controls neuronal stem cell lineages by inhibiting Deadpan and Zelda

Ilka Reichardt[1,†], François Bonnay[1,†], Victoria Steinmann[1], Inga Loedige[2], Thomas R Burkard[1], Gunter Meister[2] & Juergen A Knoblich[1,*]

Abstract

The TRIM-NHL protein Brain tumor (Brat) acts as a tumor suppressor in the *Drosophila* brain, but how it suppresses tumor formation is not completely understood. Here, we combine temperature-controlled *brat* RNAi with transcriptome analysis to identify the immediate Brat targets in *Drosophila* neuroblasts. Besides the known target Deadpan (Dpn), our experiments identify the transcription factor Zelda (Zld) as a critical target of Brat. Our data show that Zld is expressed in neuroblasts and required to allow re-expression of Dpn in transit-amplifying intermediate neural progenitors. Upon neuroblast division, Brat is enriched in one daughter cell where its NHL domain directly binds to specific motifs in the 3′UTR of *dpn* and *zld* mRNA to mediate their degradation. In *brat* mutants, both Dpn and Zld continue to be expressed, but inhibition of either transcription factor prevents tumorigenesis. Our genetic and biochemical data indicate that Dpn inhibition requires higher Brat levels than Zld inhibition and suggest a model where stepwise post-transcriptional inhibition of distinct factors ensures sequential generation of fates in a stem cell lineage.

Keywords neurogenesis; stem cells; tumorigenesis; RNA-binding protein
Subject Categories Cancer; Development & Differentiation; Neuroscience
DOI 10.15252/embr.201744188 | Received 16 March 2017 | Revised 31 October 2017 | Accepted 10 November 2017 | Published online 30 November 2017
EMBO Reports (2018) 19: 102–117

Introduction

Stem cells are characterized by the ability to generate both self-renewing and differentiating progeny. Some of them do this by segregating cell fate determinants into only one of the daughter cells during mitosis where those factors induce differentiation and prevent self-renewal. Errors in the precise regulation of this balance can cause severe stem cell overgrowth ultimately leading to tumorigenesis [1–3]. *Drosophila* larval neural stem cells, called neuroblasts (NBs), are a well-established model for investigating this regulatory mechanism [4–6]. During asymmetric cell division, NBs form apical and basal plasma membrane domains composed of distinct protein sets. Proteins in the apical domain segregate into the self-renewing cell while proteins located at the basal domain are inherited by the differentiating daughter cell where they specify cell fate identity. The Notch inhibitor Numb, the transcription factor Prospero, and the translational repressor Brain tumor (Brat) have been identified as key components of this basal domain [7–9]. The absence of these factors disturbs neuronal tissue homeostasis and leads to supernumerary NBs in larval brains. Although Numb and Prospero are well understood [10–12], the precise molecular function of Brat in NBs is currently unclear.

Drosophila NBs are subdivided into type 0, type I, and type II. Type 0 NBs self-renew and generate a post-mitotic differentiating neuron [13,14]. Type I NBs self-renew and generate ganglion mother cells (GMCs), which divide terminally into two neurons or glia cells. Type II NBs also self-renew, but they generate a transit-amplifying pool of intermediate neural precursors (INPs) to expand the pool of neurons [15–17]. All NBs express Deadpan (Dpn), a basic helix-loop-helix (bHLH) transcriptional repressor related to vertebrate Hes transcription factors [18,19]. Newly born immature INPs (imINPs) first switch off Dpn expression and then turn on another transcription factor called Asense (Ase). Finally, imINPs reinitiate Dpn expression and resume asymmetric division and are then called mature INPs (mINPs) [15–17,20,21]. In *brat* mutants, immature INPs fail to reinitiate Ase and Dpn expression. Instead, they enter a transient cell cycle block and ultimately revert to type II NBs. As a result, they form excessive NBs and ultimately a lethal transplantable brain tumor [17,21,22].

Multiple functions for Brat have been demonstrated outside the nervous system. Brat belongs to the TRIM-NHL family of proteins. It contains two B-boxes and a coiled-coil domain at the N-terminus and a C-terminal NHL domain [23]. Most *brat* alleles carry mutations in the NHL domain, indicating that this domain is functionally important [9,17,23]. The NHL domain binds the adaptor protein Miranda (Mira) and the cap-binding protein d4EHP, an inhibitor of translation [19,24]. Brat is required for establishment of the anterior–posterior body axis by repressing translation of the posterior determinant *hunchback* (*hb*) [25]. For this, it forms a protein complex with Nanos (Nos) and Pumilio (Pum) that binds to the *hb*

1 Institute of Molecular Biotechnology of the Austrian Academy of Sciences (IMBA), Vienna, Austria
2 Laboratory for RNA Biology, Biochemistry Center Regensburg (BZR), University of Regensburg, Regensburg, Germany
*Corresponding author. Tel: +43 1 79044 4800; E-mail: juergen.knoblich@imba.oeaw.ac.at
†These authors contributed equally to this work

3′UTR and inhibits translation. Brat also regulates stem cell self-renewal in the germline by repressing *mad* and *dmyc* mRNA together with Pum [26]. Recently, it was shown that Brat can also contact mRNA independently of Pum through a specific RNA motif [27–29]. Brat can also interact with the RISC-complex member Argonaute-1 [30], but unlike for other TRIM-NHL proteins, a role for Brat in the micro-RNA pathway has not been found.

How Brat acts in neural stem cell lineages is not completely understood. Brat was suggested to specify INPs by attenuating beta-catenin/Armadillo activity and thereby inhibiting the self-renewal factor Klumpfuss (Klu) [21,31]. How this would work molecularly, however, is unclear. To identify the molecular function of Brat in INPs, we developed a screening assay for the earliest transcripts whose abundance changes in *brat* mutants. We identified Zelda (Zld), previously known as *vielfältig* [32], a zinc-finger protein and key activator of early zygotic transcription [33]. Zld marks genomic regions in early *Drosophila* embryos for subsequent transcriptional activation during the maternal-to-zygotic transition (MZT) [34,35]. Zld is also involved in wing development [36], but a function in the nervous system has not been described. We show here that Zld is expressed in NBs and allows Dpn re-expression in mature INPs to promote transit-amplifying cell division. In *brat* mutants, Zld expression is sustained and promotes tumor formation and metastatic growth. We also demonstrate that Brat directly binds to the motif (A/U)UGUU(A/G/U) present in the 3′UTRs of both *zld* and the self-renewal factor *dpn* and represses their translation. Interestingly, repression of Zld and Dpn requires different levels of Brat: While low levels of Brat are sufficient to repress Zld, higher Brat levels are required for Dpn repression. We propose a model where different protein concentrations of Brat might regulate progression of the type II NB lineage.

Results

Transcriptome and rescue analysis reveals Zelda as a potential Brat target

To identify new Brat targets involved in brain tumor formation, we analyzed the transcriptome changes that occur in type II NB lineages upon *brat* RNAi over time. The *brat* RNAi phenotype corresponds to that of a null allele as Dpn is not repressed (Appendix Fig S1A) and ectopic NBs are formed. To identify the very first mRNA changes, we used the temperature-sensitive Gal4/Gal80 system to induce *brat* RNAi in a temporally controlled manner [37] (Fig 1A). 72 h after *brat* RNAi induction, cell numbers in type II NB lineages are significantly increased when compared to control lineages (Fig 1B, Appendix Figs S1B and S2). 24 h after *brat* RNAi induction, however, cell numbers in NB lineages were still the same as in wild-type, although Dpn was already misexpressed (Fig 1B, Appendix Figs S1B–D and S2). Consistently, expression of cell cycle inducers such as Cyclin E, string, E2F transcription factor was unchanged, whereas the cell cycle inhibitor dacapo was moderately increased (Appendix Fig S1G). We isolated mRNA from FACS-sorted control and 24-h *brat*-depleted type II NB lineages. The FACS protocol was optimized for maintaining a similar cell-type composition (Appendix Fig S1E). Deep sequencing identified 41 upregulated and 38 downregulated genes upon *brat* RNAi (FDR1.1; log2 fold change > 0.8; FPKM > 50; Fig 1C, Dataset EV1, Appendix Fig S1F). Among the upregulated genes were five transcription factors, all of which could be confirmed by qRT–PCR (Fig 1D). Besides Dpn and dMyc, which are known to be misregulated in *brat* mutants [9,22], these included the transcription factor Zld [32–35]. When inhibited by RNAi together with *brat*, *dpn* and *zld* were the most potent suppressors of adult lethality, suggesting that they might be the most relevant targets of Brat (Fig 1E).

brat tumor growth is impaired upon Zelda knockdown

To characterize the role of Zld in tumorigenesis, we analyzed *brat zld* tumors on three key characteristics: (i) primary brain tumor growth, (ii) lack of differentiation, and (iii) potential for unlimited proliferation. (i) Brain tumors formed upon *brat* RNAi mainly consist of dividing Mira-positive ectopic type II NB-like cells that invade most of the central brain and expand its size. We quantified *brat* tumor growth by Western blot analysis of Mira and type II NB-specific GFP expression (worGal4, aseGal80 > UAS-CD8-GFP) and observed a significant tumor reduction in *brat zld* double RNAi compared to *brat* RNAi (Fig 2A). Consistently, *brat zld* double RNAi adults developed significantly reduced tumors compared to *brat* RNAi (Fig 2B, Appendix Fig S3). As a positive control, *brat dpn* double RNAi adults developed reduced tumors to an even higher extent, further confirming the importance of Dpn expression in *brat* tumor growth (Appendix Fig S3). (ii) *brat* RNAi leads to the formation of ectopic type II NB-like cells that maintain a high-Dpn, low-Ase expression pattern (Fig 2C, middle column panels). Upon *brat zld* double RNAi, however, ectopic NBs expressed both Dpn and Ase or even Ase alone, indicating partial differentiation of these cells (Fig 2C). (iii) *brat* tumors can undergo unlimited growth and metastasis when transplanted into an adult host [1]. To further characterize *zld* as a tumor-promoting factor, we developed a method that allows the quantification of transplanted tumor growth. For this, we injected tumors formed upon *brat* single or *brat zld* double RNAi into the thorax of wild-type host flies and assessed their metastatic growth in real time by following tumor-encoded RFP. Injected *brat zld* RNAi tumor cells were still able to form metastasis but with much slower kinetics when compared to *brat* RNAi (Fig 2D and E). We conclude that simultaneous inhibition of Zld reduces the severe overgrowth phenotype observed in *brat* tumors by inducing differentiation of the ectopic NBs. Our data show that Zld contributes to *brat* tumor formation and metastatic growth and suggest that Zld might be an additional target for Brat-mediated repression in imINPs.

Zelda is required for NB lineage formation

To investigate the role of Zld in type II NB lineages, we used two independent *zld* RNAi constructs (*zld* IR and *zld* shmiR). Like their wild-type counterparts, *zld* IR or *zld* shmiR type II NBs gave rise to Ase-negative imINPs, which maturated into Ase-positive imINP (Appendix Fig S6A). In contrast to wild-type Ase-positive imINPs however, the mutant cells often failed to re-express Dpn (Appendix Fig S6A and C). We could rescue this phenotype by overexpressing Zld in *zld*-depleted type II NB (Appendix Fig S4A). Additionally, restoring Dpn by overexpression in *brat zld*-depleted type II NB could rescue primary tumor growth at larval stages

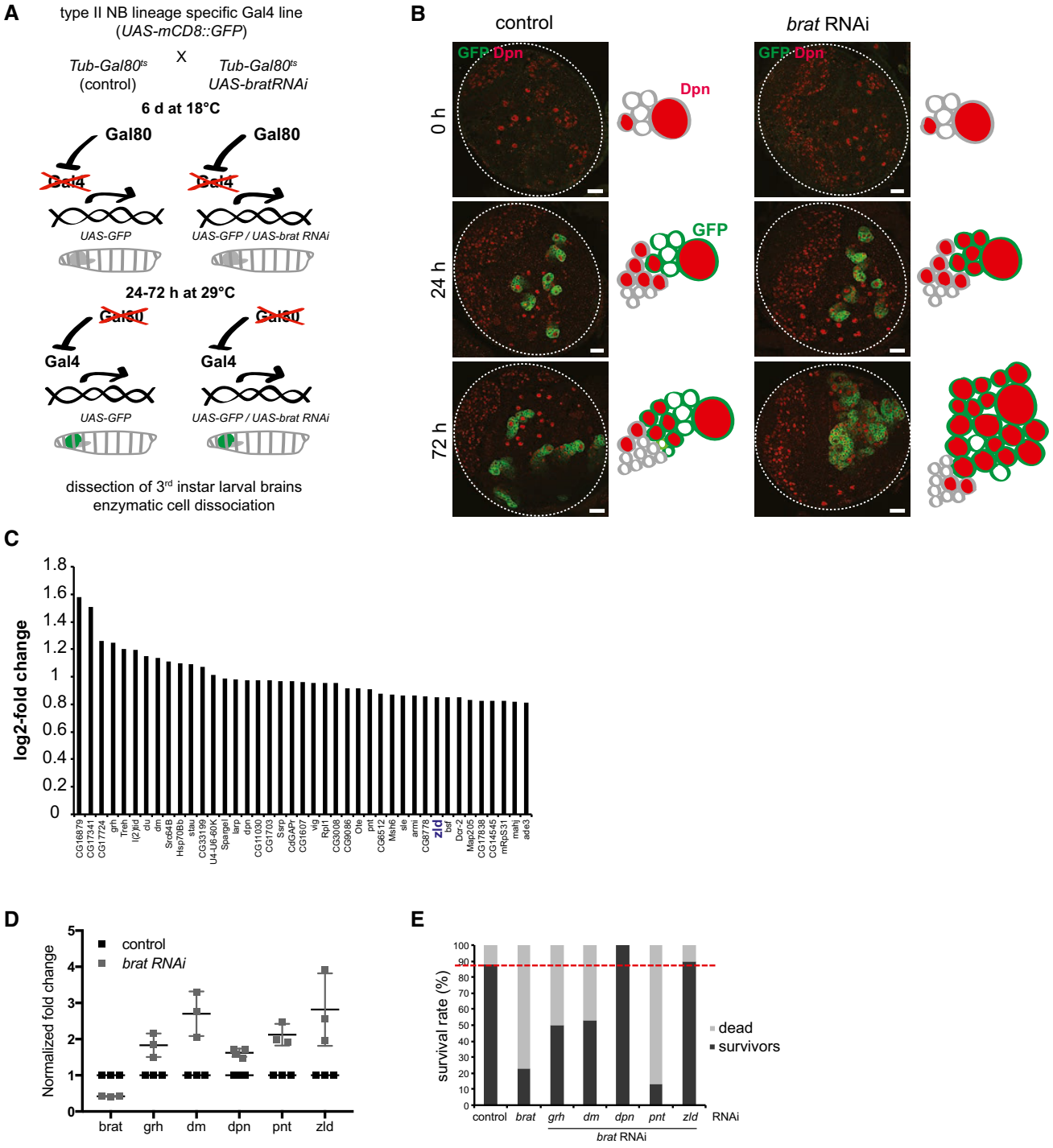

Figure 1. The transcriptional activator Zelda is a potential target of Brat.

A Cartoon illustrating the time- and tissue-specific induction of *brat* RNAi.

B Images of brain lobes expressing *brat* RNAi and/or GFP in type II NB lineages (wor-Gal4, ase-Gal80) for 0, 24, or 72 h and stained for Dpn (red). Schematics represent the images.

C Plot showing log2 fold change in the expression of candidate target genes upon *brat* RNAi (one independent experiment).

D qPCR analysis of candidate target gene expression in FACS-sorted control and *brat* RNAi type II lineages (induced with wor-Gal4, ase-Gal80) after 24 h of induction.

E *brat* rescue analysis of candidate target genes (one independent experiment). Survival rate of controls and double RNAi experiments (induced with wor-Gal4, ase-Gal80) was determined 2 weeks after adult hatching. Red dashed line indicates the survival rate of the control.

Data information: Pictures and plots are representative of three independent experiments if not otherwise indicated. Error bars represent standard deviation. Scale bars, 20 μm. See also Appendix Figs S1 and S2.

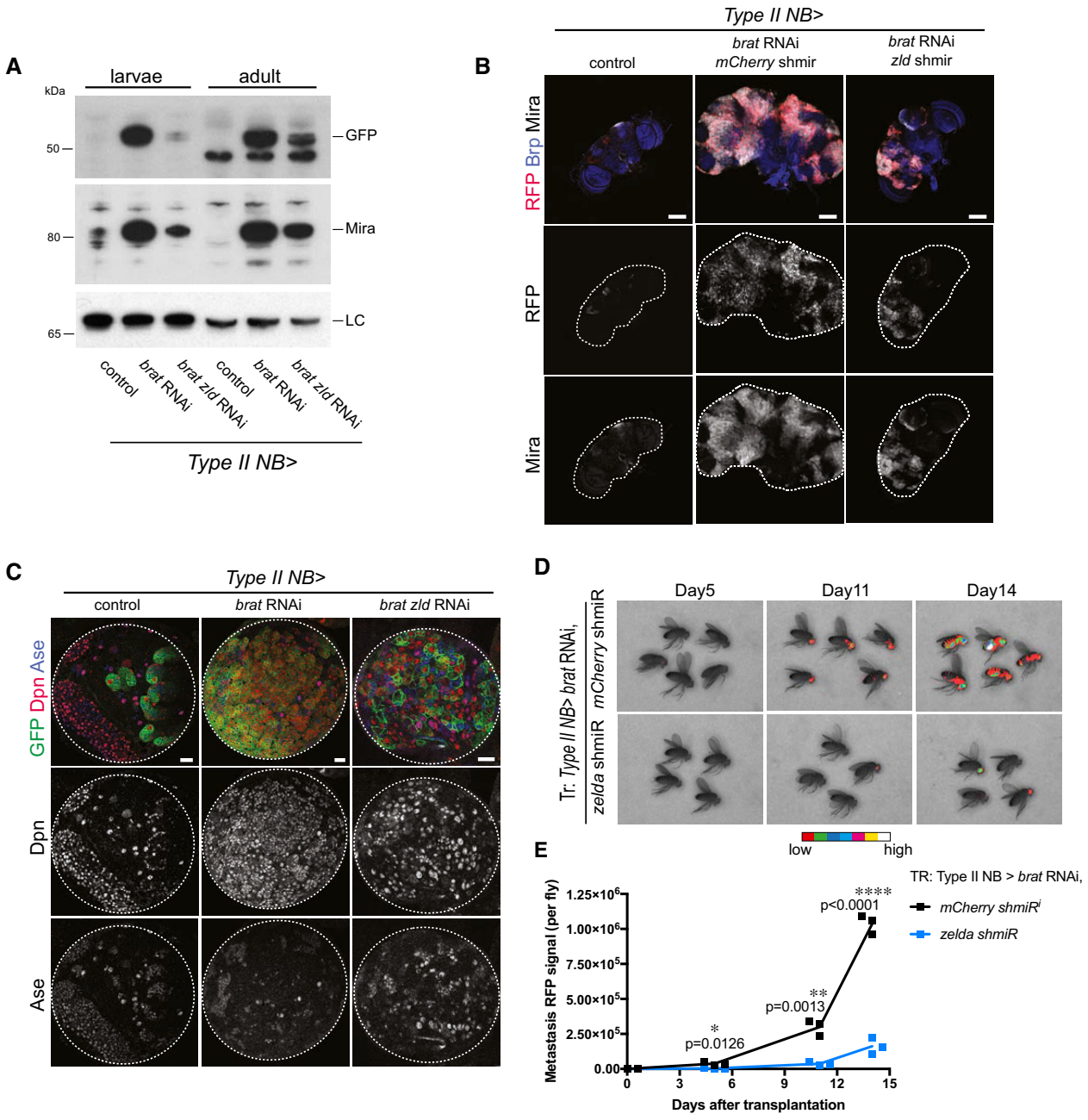

Figure 2. Zelda contributes to *brat* tumor formation.

A Western blot analysis of larval and adult brain tumors. *brat* tumors display high Mira and GFP levels, whereas upon *brat zld* double RNAi Mira and GFP levels are reduced in both larval and adult brains compared to control. LC, loading control lamin.

B Images of adult brains of control, *brat* RNAi *mCherry* shmiR and *brat* RNAi *zld* shmiR (all isoforms) (induced with wor-Gal4, ase-Gal80). Type II NB lineages are marked with stinger-RFP (red). Brains are stained for Bruchpilot (Brp, blue) and Mira (white). *brat* RNAi adult brains are overgrown by Mira-positive NB-like cells, whereas upon *brat zld* double knockdown tumors are reduced in size (images are representative of two (control) to three (other conditions) independent experiments).

C Images of larval brain lobes of control, *brat* RNAi and *brat zld* double RNAi (induced with wor-Gal4, ase-Gal80). Type II NB lineages are marked with membrane-bound GFP (green). Brains are stained for Dpn (red) and Ase (blue). *brat* RNAi tumors contain almost only GFP-positive Dpn-positive NB-like cells, whereas upon *brat zld* double RNAi tumors contain GFP-marked cells positive for Dpn or Ase, or Dpn and Ase.

D, E Real-time tumor metastasis burden after transplantation of brains expressing nuclear RFP, *brat* RNAi, *mCherry* shmiR (upper panels) and *zld* shmiR (lower panels) from type II NB driver wor-Gal4, ase-Gal80. ~4,000 RFP-positive cells were injected and RFP signal from whole fly was quantified 5, 11, and 14 days afterward. First metastasis only appeared 6 days later from *brat zld* RNAi brain injections (day 11 vs. day 5).

Data information: Pictures and blots are representative of three independent experiments if not otherwise indicated. Statistical analyses were done comparing *mCherry* and *zld* shmiR using *t*-test. *$P < 0.05$; **$P < 0.01$; ****$P < 0.0001$. Scale bars, 100 μm (B), 20 μm (C). See also Appendix Figs S3–S5.

(Appendix Fig S4B) and resulted in restored tumor burden at adult stages as quantified by tumor-specific RFP signal in the adult heads (Appendix Fig S4C and D). Consistently, qPCR analysis of larval brains expressing *zld* RNAi from the *inscuteable* driver confirmed that *dpn* transcript levels were significantly decreased (Appendix Fig S6B). Interestingly, phospho-H3 stainings revealed that the ability of imINPs to reinitiate mitosis was significantly reduced upon *zld* RNAi (Fig 3A and B). The inability of these imINPs to re-express Dpn is likely responsible for their underproliferation, as depleting Dpn from INPs resulted in the same phenotype (Fig 3A and B). As a result, the number of INPs was significantly decreased in *zld* RNAi (Fig 3C). Nonetheless, the sequential expression of mINPs temporal identity markers Dichaete, Grainy head, and Eyeless was similarly proportioned in *zld* RNAi compared to control INPs indicating a normal patterning of these cells (Fig 3D, Appendix Fig S6D–F).

Previous analysis has identified the *zld* transcripts *zld-RB* and *zld-RD* encoding two distinct proteins, Zld-PB and Zld-PD, respectively [38]. Zld-PD is missing three of the four C-terminal C2H2 zinc fingers that bind to the Zld target site and thus has potentially altered or non-functional DNA-binding properties [33,38,39]. NBs specifically express the active *zld-RB* isoform, whereas the inactive *zld-RD* isoform is expressed in the differentiating NB progeny [40] (Appendix Fig S7A). FISH analysis using specific probes for the two *zld* variants confirmed this expression pattern (Appendix Fig S7B and C). Importantly however, whether *zld-RD* is actually translated into functional proteins in these cells would remain to be explored. We next assessed the function of the *−RB* and *−RD* isoforms independently by performing isoform-specific RNAi in a *brat* tumor context. Unlike *zld-RB* RNAi, *zld-RD* RNAi constructs were unable to rescue *brat* tumor growth (Appendix Fig S5A–C). Furthermore, overexpressing *zld-RB* was sufficient to restore Dpn expression in *zld*-deficient type II NB lineage (Appendix Fig S4A). Altogether, these results suggest that *zld-RB* but not *−RD* is required for type II NB lineage proliferation. To distinguish Zld-PB from Zld-PD, we used CRISPR/Cas9 technology [41] to insert a V5-tag at the C-terminus of *zld-RB* (*zld-RB::V5*, Appendix Fig S7B and D). The insertion does not affect Zld function as flies homozygous for *zld-RB::V5* are viable and fertile. Zld-PB::V5 immunostainings confirmed its localization in NBs in both wild-type and *brat* mutant larval brains (Fig 3E). The specificity of Zld-PB::V5 staining was further confirmed by *zld* RNAi (Appendix Fig S7E). Detailed lineage analysis revealed that Zld-PB is exclusively present in NB but absent from INPs, with some exceptions where Zld can sometimes still be detected in recently born imINPs (Fig 3F). We observe a similar pattern for other NB-specific factors such as Dpn (Appendix Fig S9B, yellow arrow). Taken together, our data indicate that active Zld is specifically expressed in NBs and is absent from its progeny. Depleting Zld from the NB leads to a decreased number of INPs, most of which no longer express Dpn.

Brat suppresses Zld-PB by binding to its 3′UTR

We next investigated whether Zld would be a direct target of Brat. First, we performed RNA immunoprecipitation (RIP) experiments on control and $brat^{K06028}$ mutant larval brain tissue and observed that Brat can bind to *zld-RB* RNA (Fig 4A). Second, in order to investigate the regions of Brat binding within the *zld-RB* 3′UTR, we performed an electrophoretic mobility shift assay (EMSA) using the NHL domain of Brat, which was shown to bind mRNA [27], together with various overlapping *in vitro* transcribed ~150-nt-long fragments of the *zld-RB* 3′UTR (Fig 4B). Increasing amounts of recombinant Brat-NHL were incubated with ^{32}P-labeled RNA fragments and the resulting protein-RNA complexes analyzed by native gel electrophoresis (Fig 4C). Brat-NHL did not bind to *zld* RNA fragments 1, 2, 5, 6, 8, 11, 12, and 14 (Fig 4B and C; "non-binders" in black), whereas for *zld* RNA fragments 3, 4, 7, 9, 10, 13, and 15 we observed a clear shift of free RNA to RNA-protein complex at Brat-NHL protein concentrations of 50–100 nM (Fig 4B and C; "binders" in green). Interestingly, we observed an almost complete RNA shift at the respective concentrations, indicating high affinity binding. RNA binding was sequence-specific, as the protein-RNA complexes could be chased by a 1,000-fold molar excess of unlabeled binders but not by a 1,000-fold molar excess of unlabeled t-RNA, present in all reactions. *zld* RNA fragments bound by Brat contained a specific motif (A/U)UGUU(A/G/U), the Brat-binding motif. This motif is very similar to what has recently been identified as a consensus motif for Brat binding [28,29]. To test whether this motif is required for Brat binding to *zld* RNA, we generated RNA fragments harboring mutations or deletions of the Brat-binding motif (Fig 4B). Mutations or deletions of the motif sites in *zld* RNA fragments 3, 4, 7, and 9 reduced or abolished Brat-NHL binding (Fig 4D). In order to test whether the Brat-binding motif is required for the repression of *zld* RNA, we tested the mutated variants of full-length *zld-RB* 3′UTR in a *Drosophila* S2 reporter assay (Fig 4E). S2 cells were cotransfected with wild-type or mutated *zld-RB* 3′UTR and full-length Brat. While mutating individual Brat-binding sites did not interfere with Brat-mediated repression, mutation of all Brat-binding sites abolished Brat-mediated repression of the *zld-RB* 3′UTR. Taken together, our data demonstrate that Brat-NHL directly binds to sequence-specific motifs in the 3′UTR of *zld-RB*, which are required for Brat-mediated repression.

Dpn repression requires high Brat levels

Brat was previously shown to interact with *dpn* mRNA [29]. To compare its binding to *dpn* and *zld* RNA, we performed an EMSA experiment using the experimental setup described above (Fig 5A). *dpn* RNA fragments 1–3 shifted from free RNA to RNA-protein complexes at Brat-NHL concentration of 50–100 nM (Fig 5B). In contrast to *zld* RNA, *dpn* RNA shifted only partially at a Brat concentration of 50 nM, indicating that Brat binds to d*pn* RNA with lower affinity. *dpn* fragments bound by Brat contained the Brat-binding motif. Consistently, mutations of the motif sites in fragment 1 abolished Brat-NHL binding (Fig 5C). Interestingly however, mutations of these motifs in fragment 2 and 3 did not prevent Brat-NHL binding, suggesting the existence of alternative binding specificities. In order to demonstrate that Brat protein–*dpn* RNA binding can lead to Dpn repression, we co-expressed a *dpn* 3′UTR GFP reporter together with full-length Brat in *Drosophila* S2 cells. Compared to control, the *dpn* 3′UTR reporter was repressed upon Brat expression, albeit not to the same extent as the *zld* 3′UTR reporter (Fig 5D). These data suggest that the translational repression of Dpn requires higher levels of Brat than that of Zld.

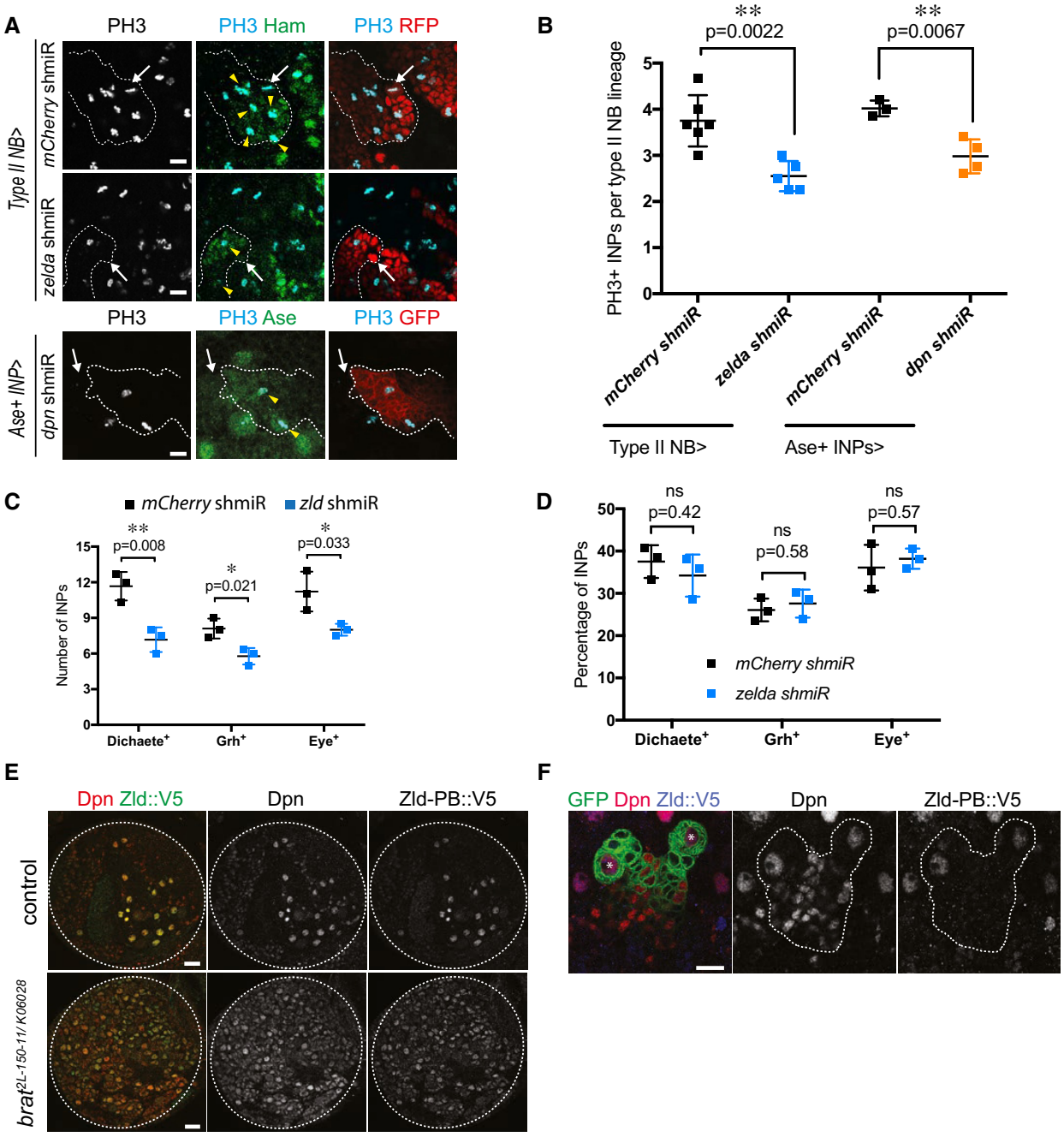

Figure 3. Zelda is required for proliferation potential, but not differentiation patterns of INPs.

A Close-up images of *mCherry* and *zld* shmiR type II NB lineages marked with nuclear RFP (red, upper panels) or membrane-bound GFP (red, lower panels) and stained for INP marker Hamlet or Ase (green) and PH3 (light blue). Note that in *zld* and *dpn* shmiR, type II NB lineages contain less proliferative INPs (yellow arrowheads). White arrows designate the position of type II NBs.

B Quantification of PH3-positive INPs in type II NB lineages expressing *mCherry* or *zld* shmiR (induced with wor-Gal4, ase-Gal80) or *mCherry* and *dpn* shmiR (induced with ase-Gal4) (three or more independent experiments).

C, D Cell count (C) and relative proportions (D) of Dichaete-, Grainy head (Grh)-, and Eyeless (Eye)-positive INPs of *mCherry* and *zld* shmiR (induced with wor-Gal4, ase-Gal80) type II NB lineages. While their global number is reduced, the proportions between each temporal state of INP is maintained in *zld* shmiR type II NB lineages.

E Brain lobes of control and $brat^{2L\text{-}150\text{-}11/K06028}$ trans-heterozygous expressing endogenous Zld-PB::V5 stained for Dpn (red) and V5 (green).

F Close-up images of type II NB lineages marked by membrane-bound GFP expressing endogenous Zld-PB::V5 stained for Dpn and V5. Note that Zld-PB::V5 is only expressed in NBs but absent from their progeny. *type I NB, **type II NB.

Data information: Pictures and plots are representative of three or more independent experiments. Error bars represent standard deviation. Statistical analyses were done using *t*-test. *$P < 0.05$; **$P < 0.01$; ns: non-significant. Scale bars, 10 μm (A, F), 20 μm (E). See also Appendix Figs S6 and S7.

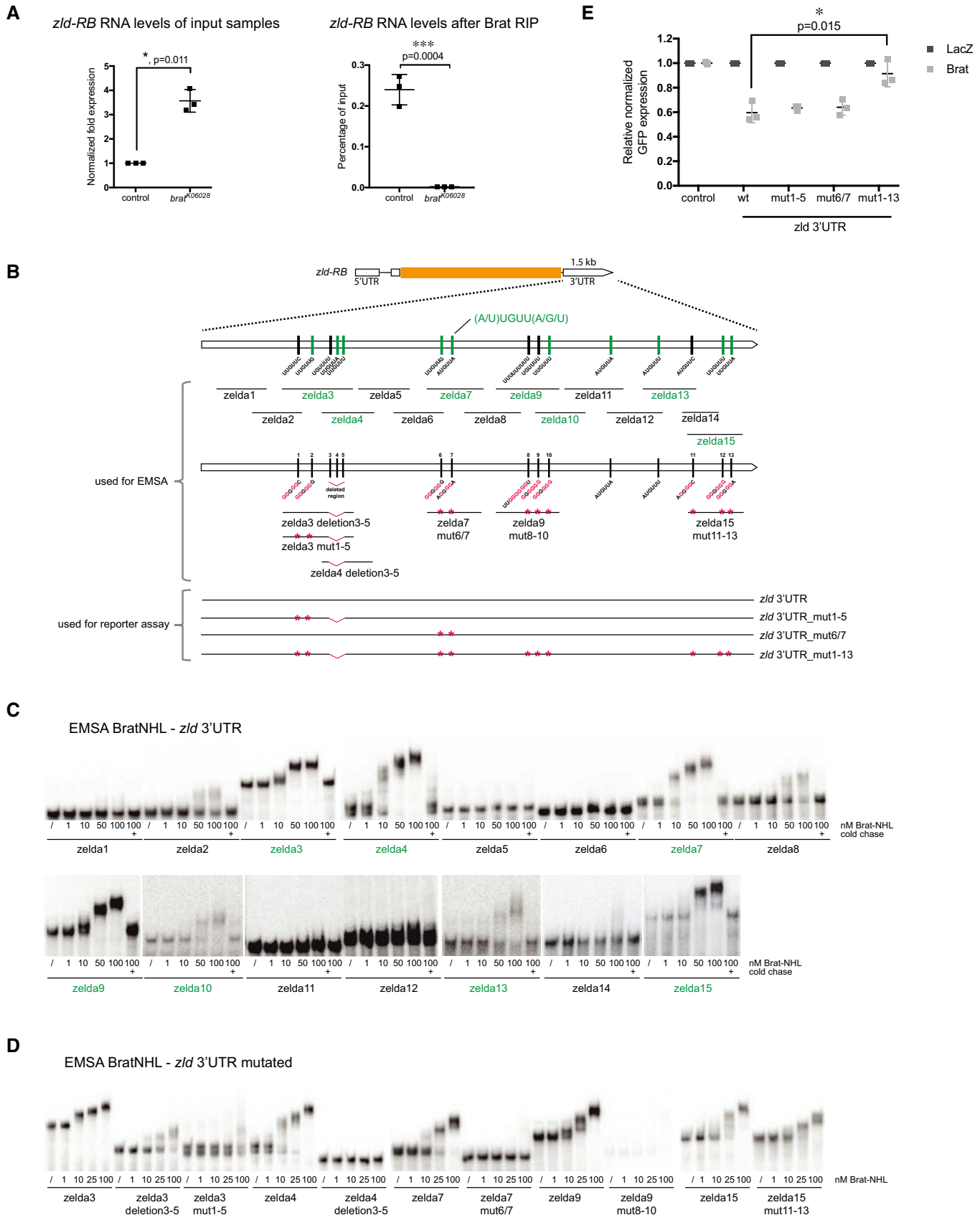

Figure 4.

brat^{G774D} mutants maintain Zld-PB but not Dpn repression in mINPs

To dissect the relative contribution of Dpn and Zld repression to Brat *in vivo* function, we used the *brat*^{fs1} allele. In *brat*^{fs1} (hereafter referred to as *brat*^{G774D}), glycine 774 in the NHL domain is replaced by Aspartate. Unlike *brat*$^{2L\text{-}150\text{-}11}$ strong loss-of-function mutants, *brat*^{G774D} mutants do not form brain tumors [19,25]. To test the effect of this mutation on Zld and Dpn repression, we analyzed *brat*^{G774D} MARCM clones. 48 h after heat-shock induced recombination, control NB clones contained one Dpn-positive NB, two to three Ase-negative imINPs, four to five Ase-positive imINPs and multiple Dpn, Ase double-positive mINPs (Appendix Fig S8A–C) [42]. Clones mutant for the strong loss-of-function allele *brat*$^{2L\text{-}150\text{-}11}$ contained multiple Dpn-positive NB-like cells and no imINPs or mINPs. *brat*^{G774D} mutant NB clones, in contrast, contained one Dpn-positive NB but lacked the first Dpn, Ase double-negative imINPs stage. Instead, we observed three to four Dpn-positive, Ase-negative cells and multiple Dpn, Ase double-positive mINPs. These Dpn-positive, Ase-negative NB daughter cells were located close to the NB and were positive for Mira (Appendix Fig S8E). Importantly, these cells were not more proliferative than WT mINPs and the overall *brat*^{G774D} clone cell numbers were comparable to WT (Appendix Fig S8F and G). Zld-PB is absent from NB progeny in controls (Fig 3F). However, although Zld-PB continued to be expressed in *brat* null mutant clones, it was still repressed in *brat*^{G774D} mutant imINPs (Fig 5F). Thus, *brat*^{G774D} can still repress Zld-PB but can no longer repress Dpn.

We next aimed to explore the molecular mechanisms underlying the *brat*^{G774D} mutant phenotype. Brat^{G774D} fails to successfully integrate into the Nos/Pum/RNA complex [25]. Brat^{G774D} also no longer binds to the adaptor protein Mira [19] and therefore cannot localize asymmetrically during NB division (Fig 5E) and is no longer enriched in imINPs. The *brat*^{G774D} phenotype could be due to the failure of Brat^{G774D} to interact with Pum. However, Zld-PB expression was normal upon *pum* knockdown or in *pum*^{ET1} type II NB clones (Appendix Fig S8D). In addition, neither *pum* RNAi nor *pum*^{ET1} clones affected Dpn repression in imINPs (Appendix Fig S11B), indicating that Brat-mediated Dpn and Zld repression is Pum-independent. Alternatively, the *brat*^{G774D} phenotype could be explained by the inability of Brat^{G774D} to segregate asymmetrically, which would result in lower Brat levels in INPs that are sufficient to repress Zld-PB but no longer repress Dpn. To test this possibility, we overexpressed Brat^{G774D} in NBs and analyzed Dpn expression. Consistently, overexpressing wild-type Brat and Brat^{G774D} in NBs both strongly reduced Dpn expression indicating that Brat^{G774D} is still capable of repressing Dpn at high protein levels (Fig 5G). We also generated *brat* RNAi-resistant constructs to test the ability of Brat^{G774D} to rescue tumor formation in a *brat* RNAi background. Overexpressing wild-type Brat and Brat^{G774D} both rescued *brat* tumor formation (Fig 5G, Appendix Fig S11C). Taken together, these data suggest that the lack of Dpn repression in *brat*^{G774D} mutants is due to the defect in asymmetric segregation.

Low Brat levels repress Zld but not Dpn in mINPs

Our results prompted us to test whether the differential activity of Brat toward Zld and Dpn is important for lineage specification. Previous experiments have revealed that Brat levels decrease during INP maturation (a period of 5–6 h [43]). Upon NB division, Brat was highly concentrated in imINPs, but only around 40% of the protein level was still present in Dpn-positive mINPs (Fig 6A, Appendix Fig S9A–C). Consistently, analysis of heat-shock induced Brat expression showed that protein levels were maximal 1 h after heat shock but strongly reduced 5–10 h after the heat shock (Fig 6B). Thus, Brat protein turnover roughly corresponds to the time of INP maturation. This suggests the intriguing possibility that the decrease in Brat protein levels during INP maturation might allow re-expression of Dpn but not Zld in mINPs.

To support this hypothesis, we used two experimental approaches to titrate Brat levels in INPs. First, we performed *brat* RNAi in the type II NB progeny using the erm-Gal4 driver (3rd chromosome). Indeed, *brat* RNAi in Ase-positive imINPs was sufficient to partially lift Zld repression in INPs (Fig 6C–E). In a second approach, we used a Myc-tagged Brat construct (Myc-Brat) that allowed us to follow Brat protein levels and Dpn and Zld suppression simultaneously in INPs. When expressed from the *erm-Gal4* driver (3rd chromosome), this construct resulted in high levels of Myc-Brat in both Ase-positive imINPs and young mINPs (Fig 6F and G). Due to high Brat protein turnover, however, Myc-Brat levels decreased in older mINPs that are located further away from the NB. As a consequence, young mINPs with high levels of Myc-Brat showed low Dpn levels whereas older mINPs with lower Myc-Brat levels had twofold higher Dpn levels (Fig 6F and G). Altogether, these data suggest that the decrease in Brat protein levels during INP maturation allows re-expression of Dpn but not Zld-PB in mINPs.

Discussion

Our data suggest a molecular mechanism through which the tumor suppressor Brat could perform its function in type II NB lineages.

Figure 4. Brat directly targets the 3′UTR of *zld* via a specific binding motif.

A qPCR analysis of *zld-RB* transcript after Brat-RIP of control and *brat*^{K06028} mutant larval brain tissue. Left diagram represents *zld-RB* RNA levels of the Input. Right diagram represents *zld-RB* RNA levels after Brat-RIP experiment.

B Schematic representation of *zld-RB* locus and the *zld-RB* 3′UTR fragments used in this study. Sites of the Brat-binding motif within the *zld-RB* 3′UTR are highlighted. Fragments which bind to Brat-NHL are labeled in green; non-binding fragments in black. Nucleotide mutations and deletions are marked in red.

C, D Recombinant Brat-NHL was incubated with ^{32}P-labeled wild-type (C) or mutated (D) *zld* RNA fragments as indicated and analyzed by native gel electrophoresis. Note that mutations of the Brat-binding sites in the *zld-RB* 3′UTR greatly impair RNA binding of Brat-NHL.

E *Drosophila* S2 cells were cotransfected with GFP-*zld-RB* 3′UTR reporters as indicated together with full-length Brat. RFP was used as a transfection control; LacZ was used as an overexpression control. Note that repression of GFP-*zld-RB* 3′UTR reporter bearing all Brat-binding site mutations is greatly reduced.

Data information: Pictures and blots are representative of three independent experiments. Error bars represent standard deviation. Statistical analysis was done using *t*-test. *$P < 0.05$; ***$P < 0.001$.

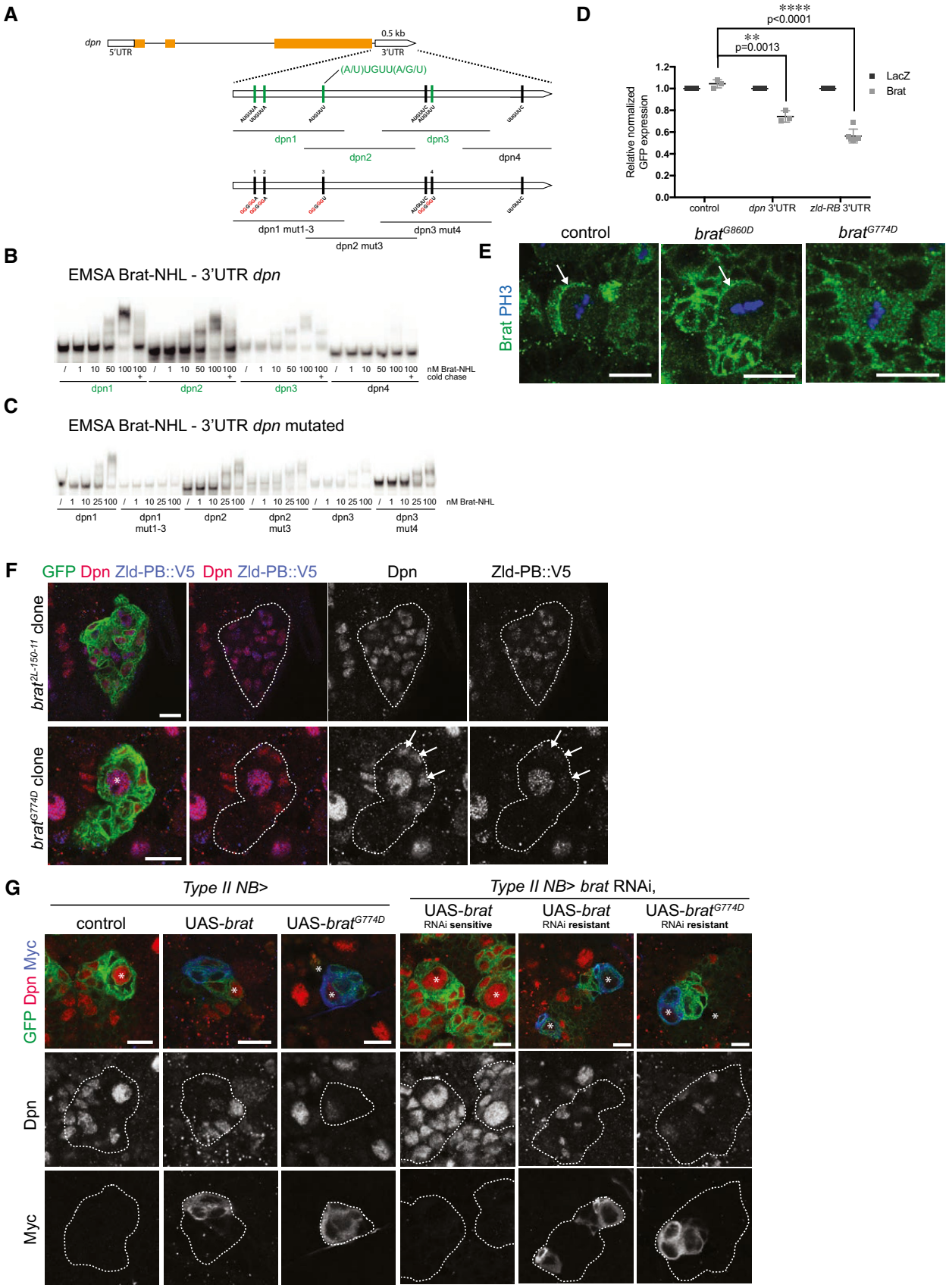

Figure 5.

Figure 5. Brat represses its targets in a concentration-dependent manner in INPs.

A Schematic representation of *dpn* locus and the *dpn* 3′UTR fragments used in this study. Sites of the Brat-binding motif within the *dpn* 3′UTR are highlighted. Fragments which bind to Brat-NHL are labeled in green; non-binding fragments in black. Nucleotide mutations and deletions are marked in red.

B, C Recombinant Brat-NHL was incubated with ^{32}P-labeled wild-type (B) or mutated (C) *dpn* RNA fragments as indicated and analyzed by native gel electrophoresis. Note that mutations of the Brat-binding sites in the *dpn* 3′UTR greatly impair RNA binding of Brat-NHL.

D *Drosophila* S2 cells were cotransfected with GFP-*dpn* 3′UTR or GFP-*zld-RB* 3′UTR reporters as indicated together with full-length Brat. RFP was used as a transfection control; LacZ was used as an overexpression control.

E Close-up images of larval brain NBs stained for PH3 (blue) and Brat (green). In control and $brat^{G860D}$ mutant NBs Brat localizes asymmetrically during mitosis (arrows), whereas in $brat^{G774D}$ mutants Brat remains ubiquitously distributed.

F Close-up images of $brat^{2L\text{-}150\text{-}11}$ or $brat^{G774D}$ mutant type II NB lineages marked by membrane-bound GFP expressing endogenous Zld-PB::V5 and stained for Dpn (red) and V5 (blue). White arrows indicate immature INPs failing to repress Dpn but not Zld-PB in a $brat^{G774D}$ clone.

G Close-up images of type II NBs marked with membrane-bound GFP expressing with wor-Gal4, ase-Gal80, (left panels) Myc-tagged wild-type *brat*, or $brat^{G774D}$ or (right panels) RNAi-sensitive or RNAi-resistant Myc-tagged Brat constructs together with *brat* RNAi and stained for Dpn (red) and Myc (blue). Asterisks designate type II NB.

Data information: Pictures and blots are representative of three independent experiments. Error bars represent standard deviation. Statistical analyses were done using *t*-test. $^{**}P < 0.01$; $^{****}P < 0.0001$. Scale bars, 10 μm. See also Appendix Figs S8–S10.

We first demonstrate that the transcription factor Zld, in addition to Dpn, is a critical target of Brat-mediated translational repression. Via its NHL domain, Brat directly binds to the *dpn* and *zld* 3′UTRs and represses translation via a sequence-specific binding motif. Several results suggest that distinct levels of Brat are required to suppress these two targets: First, we demonstrate that $brat^{G774D}$, a hypomorphic mutant quantitatively attenuated in imINPs, is able to repress Zld but not Dpn, but can suppress both targets upon overexpression. Second, we demonstrate that Dpn repression correlates with high Brat protein levels, both in wild-type imINPs as well as upon overexpression. Finally, we demonstrate that Brat binds to *dpn* RNA with lower affinity than to *zld* RNA. Together, our data suggest a model (Fig 6H) where high Brat protein levels repress both *dpn* and *zld* RNA in young imINPs immediately after asymmetric cell division. Over time, Brat levels decline allowing for the re-expression of Dpn but not Zld in INPs. Importantly, our data do not exclude that pre- or co-transcriptional regulation of these factors would occur in parallel of Brat-mediated post-transcriptional control.

What could be the role of a Brat level-dependent inhibition mechanism during type II NB lineage progression? Dpn is well known to be a crucial factor supporting self-renewal in NB [44–46] and needs to be repressed in imINPs to prevent reversion into tumor NB-like cells (illustrated in Appendix Fig S11A). Our data further demonstrate that decreasing Brat levels in mINPs are crucial to allow Dpn re-expression, which is essential to reinitiate cell division (Fig 3A and B). We have identified Zld as a crucial determinant allowing this re-expression in INPs. For this, Zld seems to act in type II NBs where its active isoform is expressed but seems dispensable in INPs, where its levels are continuously repressed by Brat (Fig 6C–E).

Importantly however, artificially re-establishing Zld expression in INPs does not result in ectopic NB formation in a wild-type or $brat^{G774D}$ background (data not shown). This can be explained by two possibilities. First, although Zld-PD cannot activate transcription and lacks the relevant domains [39], its RNA is expressed in the NB progeny and could potentially antagonize Zld-PB function. Whether Zld-PD is actually translated into functional proteins in these cells would remain to be explored. However, it has been shown that co-expression of Zld-PA (identical to PB) and Zld-PD significantly reduced gene expression, demonstrating that Zld-PD acts dominantly to suppress Zld-mediated transcriptional activation. This was explained by competition of the two isoforms for interaction with cofactors required to activate transcription [39]. Second, it is possible that low Brat levels maintain the repression of one or several—yet to be characterized—key factors in addition to Zld. Our RNA-seq data and *brat* lethality suppression assay highlighted *dm* and *klu* as potential additional targets of Brat repression. Thus, the protein level-dependent Brat-mediated inhibition mechanism allows

Figure 6. High Brat levels are required to repress Dpn.

A Close-up images of larval brains expressing *brat* shmiR and membrane-bound GFP from type II NB driver (wor-Gal4, ase-Gal80) and stained for Dpn (red) and V5-Brat (blue). Yellow arrows and arrowheads indicate Dpn-negatve immature INPs and Dpn-positive mature INPs, respectively.

B Western blot analysis showing Brat protein turnover. Flies expressing Brat under control of the heat-shock promoter (hs-*brat*) were heat-shocked for 1 h and Brat expression was determined at indicated time points after heat shock. Note that around 1 h Brat expression reaches its maximum and after 5–10 h, the expression level is strongly reduced.

C Close-up images of type II NB lineages expressing endogenous V5-tagged Zld-PB and expressing membrane-bound GFP, *mCherry,* or *brat* shmiR from Ase$^+$ INPs driver (erm-Gal4, 3rd chromosome) stained for Dpn and V5 (red). Note *brat* shmiR INPs re-express Zld-PB::V5 (yellow arrows) compared to *mCherry* shmiR INPs (white arrows).

D Quantification of Zld-PB::V5 signal (intensity normalized by the INPs' outlined surface, ImageJ) from *mCherry* and *brat* shmiR Dpn-positive INPs per lineage.

E qPCR analysis of *Ase* (negative control), *zld* and *dpn* transcripts after *brat* RNAi in FACS-sorted Ase$^+$ INPs (erm-Gal4, 3rd chromosome).

F Close-up images of type II NB lineages expressing membrane-bound GFP and myc-tagged Brat from the Ase-positive imINP driver (erm-Gal4 on the 3rd chromosome) and stained for Dpn (red) and Myc. mINPs expressing high (arrowheads) and low (arrows) Myc-Brat are indicated.

G Quantification analysis of Dpn fluorescence intensity measurements in mature INPs expressing high levels of Myc-Brat (closer to the NB) vs. in INPs expressing low levels of Myc-Brat (more distant to the NB). White asterisks indicate type II NB.

H Model of Brat-mediated repression of Zld and Dpn in type II NB lineages.

Data information: Pictures and blots are representative of three independent experiments. Error bars represent standard deviation. Statistical analyses were done using *t*-test. $^{*}P < 0.05$; $^{**}P < 0.01$; $^{***}P < 0.001$. Scale bars, 10 μm. See also Appendix Fig S11.

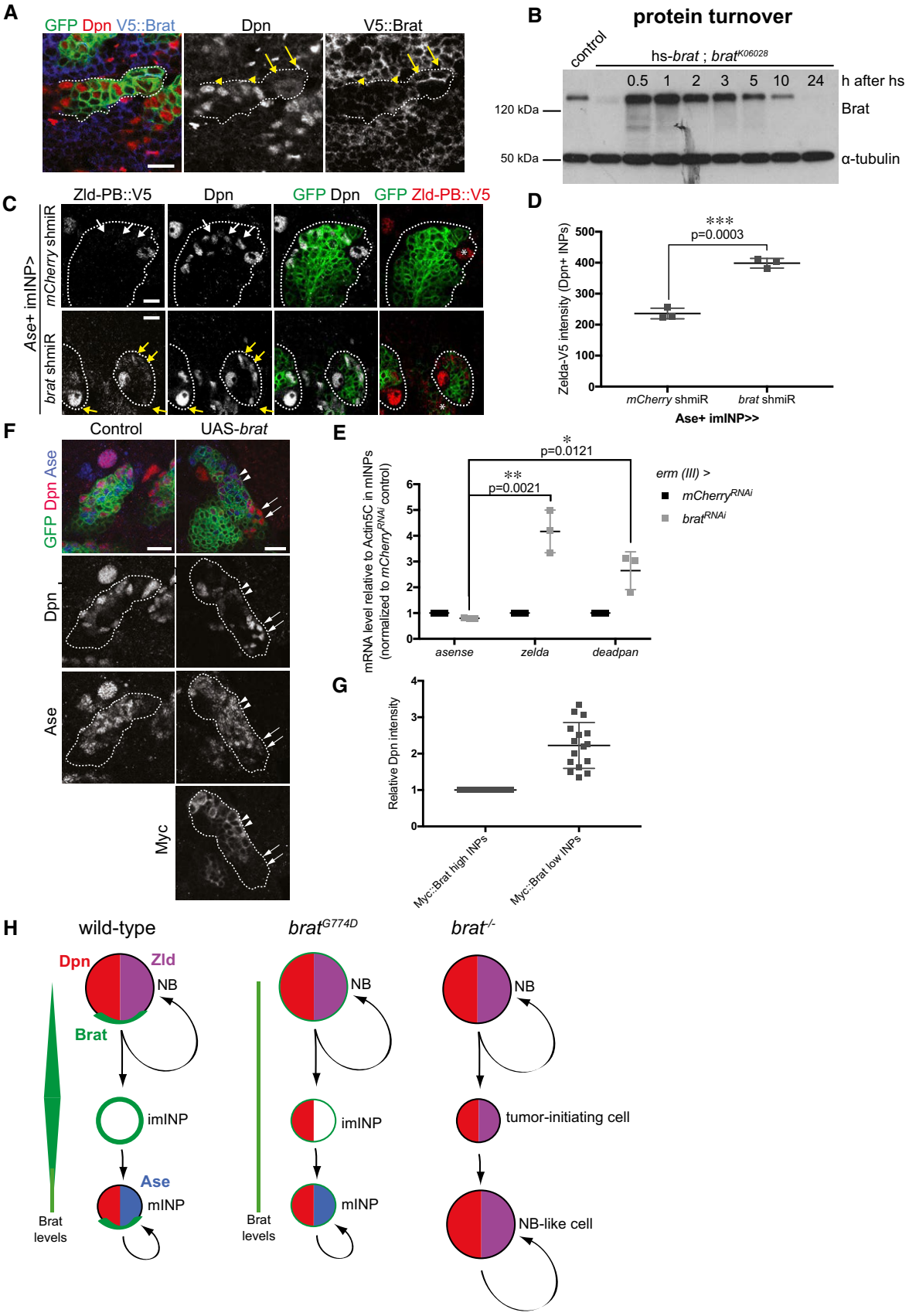

Figure 6.

a tightly regulated repression machinery during INP cell fate specification and prevents INPs from reverting into ectopic NBs.

Brat does not repress Zld in NBs although it is expressed there. It is possible that an inhibitor or a specific post-transcriptional modification prevents Brat from acting in NBs. Alternatively, Brat levels normally present in the NBs are too low for translational target gene repression. In INPs, both asymmetric segregation and transcriptional upregulation increase Brat levels and target genes are repressed. Why are *zld* and *dpn* RNA differentially sensitive to Brat levels? Brat directly binds to sequence-specific motifs in the *zld* and *dpn* 3′UTR. While the *zld* 3′UTR contains 10 motif sites, *dpn* 3′UTR contains only 4. It is possible that the abundance of motif sites within a 3′UTR determines the efficiency of Brat binding and that with a higher number of motif sites within the 3′UTR, the Brat-binding affinity increases.

What is the molecular activity of Zld in NBs? Zld can bind to the TAGteam elements, which are highly distributed among the genome. Also, Zld was shown to bind to the *dpn* locus, which contains two TAG motifs in the promoter region and seems to regulate Dpn expression in larval brains. Surprisingly, however, removing Zld only weakly interferes with Dpn expression in the NB, whereas it has very strong consequences for Dpn expression in INPs resulting in their underproliferation. This result is very surprising as the presumably active Zld-PB protein is present in NBs but not in mINPs. It is possible that Zld-PD has an active role in the NB progeny. However, it has been demonstrated very nicely that all four zinc fingers are required for TAGteam binding and that Zld-PD lacking three of the four zinc fingers fails to activate transcription [39]. We also cannot exclude that levels of Zld-PB undetectable with our reagents repress Dpn in INPs. More likely, however, Zld interacts with loci such as Dpn in NBs to license it for transcription. This function would be analogous to what has been described for early embryos where Zld binds to its target regions long before they are transcribed during MZT [34]. In this scenario, Zld would modify the its target loci in NBs so that transcription can be re-initiated in mINPs once Brat levels have declined.

Our transcriptome data showed that genes bearing at least one Brat-binding motif were significantly enriched among the genes repressed by Brat in type II NB lineages (FDR1.1, FPKM > 1, log2 fold change 1; Appendix Fig S10A). Thus, RNAs harboring a Brat-binding motif are preferentially repressed in INPs and we suggest that Brat may target a number of genes other than *dpn* and *zld* for translational repression. It was proposed that Brat also antagonizes Klu and Arm in imINPs [31]. Klu is a self-renewal factor whose 3′UTR contains three Brat-binding motifs, and we cannot exclude that it serves as an additional target for Brat.

How does Brat mediate translational repression? Brat can repress *hb* RNA in a complex with Pum and Nos [25]. We show that repression of Dpn or Zld is not altered in *pum* knockdown or *pum* mutant clones. This is consistent with what has recently been described for Brat function during embryogenesis [28] and is also supported by our observation that the known Brat/Pum target Nos cannot be detected in NB lineages [40]. Thus, Brat most likely acts in NB lineages through a mechanism independent of the Pum/Nos complex. Brat can interact with the cap-binding protein d4EHP, which inhibits translation by binding the mRNA 5′ cap structure [24,47]. Mutations of amino acid G860, R837 and K882 in the Brat-NHL domain reduce or abolish interaction with d4EHP [24]. While $brat^{G860D}$ no longer represses Dpn, $brat^{R837D}$ and $brat^{K882E}$ still do (Appendix Fig S10B) suggesting that d4EHP binding is not crucial for this activity. Similar results have been previously obtained for Brat-mediated repression of *hb* [27]. Brat also binds Not1, a subunit of the CCR4-Not complex catalyzing mRNA deadenylation [48]. It is possible that Brat-mediated translational repression is accompanied by recruitment of CCR4/Not to promote RNA degradation. The translational repressor Smaug [49–51] has been shown to recruit CCR4/Not to trigger maternal transcript destabilization, and it is plausible that Brat and Smaug act together in translational repression during INP cell fate specification.

The self-renewing capacity of INPs differs from that of NBs. While NBs divide up to 30 times during their life span, INPs undergo only five to eight rounds of division. So far, all known self-renewing factors in NBs are first repressed in imINPs but reappear in mINPs (Dpn, N, Klu, HLHmgamma). To our knowledge, active Zld-PB is the first factor common to all NBs (type I and type II) that is not re-expressed in INPs but crucial for their proliferation. Zld has been described as a key player in activating the genome at the MZT and to promote timely and robust transcriptional activation [34,35]. We suggest that potential activation of the Dpn locus by Zld in the NB is deactivated in older INPs so that INPs lose their self-renewing capacity over time. The same may also happen to *brat* mutant NB-like cells upon knockdown of *zld*: The *brat* tumor contains Ase-positive differentiated cells and is progressively rather than completely suppressed.

The Trim-NHL family proteins are conserved among metazoa and are known to play a role in cell fate determination. In humans, only Trim3 acts as a tumor suppressor in glioblastoma that reprograms glioma stem cells toward differentiation by suppressing *c-Myc* [52]. Also, the mammalian Trim71 promotes reprogramming of differentiated cells into induced pluripotent stem cells by inhibiting the prodifferentiation factor *EGR1* [53]. It would be worth the effort to analyze if the mechanism behind their repressive function is similar to Brat.

Similar to *Drosophila*, transit-amplifying lineages can also be found in human brain development and are thought to underlie the evolutionary expansion of the neocortex [54,55]. It would be interesting to evaluate if differences in the presence of a transcriptional activator like Zld also determine the cell behavior of the distinct cell types in human neural stem cell lineages.

Materials and Methods

Fly strains, RNAi, and clonal analysis

Drosophila stocks used in this study were *brat* RNAi [Transformant ID (TID) 31333 and 105054; Vienna Drosophila RNAi Center (VDRC)]; *grh* RNAi (TID 106879; VDRC); *dm* RNAi (TID 106006; VDRC); *dpn* RNAi (TID 106181; VDRC); *pnt* RNAi (TID 105390; VDRC); *zld* IR (TID 38706; VDRC); *brat* shmiR (BL34646); *pum* shmiR (BL36676, BL38241); *zld-RB 3′UTR* shmiR (BL42016) *dpn* shmiR (generated in this study, see below); *zld* shmiRs ["all", *−RB* and *−RD* (1, 2 and 3)] (generated in this study, see below); FRT40A; FRT40A, $brat^{2L\text{-}150\text{-}11}$ [9]; FRT40A, $brat^{fs1}$ [25]; FRT40A, $brat^{ts1}$ [23]; $brat^{K06028}$ [23]; FRT82B; FRT82B $pum^{ET\text{-}1}$ [56]; UAS-3xFlag6xMyc::*brat* constructs (generated in this study, see below); UAS-*zld-RB*

[36], UAS-*dpn* (*dpn* full-length cDNA cloned into a pUAST and inserted into attP40 site, this study); *V5::brat* (generated in this study, see below); *zld-RB::V5* (generated in this study, see below). Gal4 driver lines used were UAS-dcr1; wor-Gal4, ase-Gal80; UAS-mCD8::GFP [57]; erm-Gal4 (II); UAS-mCD8::GFP [21]; UAS-CD8::GFP; erm-Gal4 (III) [58,59]. Clones of NBs homozygous for $brat^{2L\text{-}150\text{-}11}$, $brat^{fs1}$, $brat^{ts1}$, and $pum^{ET\text{-}1}$ were generated by Flippase (FLP)/FLP recombination target (FRT)-mediated mitotic recombination, using elav-Gal4 (C155) [60]. Larvae were heat-shocked for 1 h at 37°C and dissected as wandering third-instar larvae. RNAi and shmiR crosses were set up and reared at 29°C, and wandering third-instar larvae were dissected 5 days after. For the *brat* rescue double RNAi crosses were set up and reared at 29°C. At least 10 flies of the respective genotype were collected 2 days after adult hatching, kept at 29 degrees, and recounted 2 weeks after.

Generation of shmiR lines

Efficient shRNA prediction was made by implementing an algorithm described previously [61] and modified for 22-bp shmiRs. An off-target algorithm was designed to exclude potential off-targets [62,63]. The synthesized oligos were annealed and cloned into the Walium20 vector according to the protocols of The Transgenic RNAi Project (flyrnai.org). Oligo sequences used for generating *dpn* and *zld* shmiRs are listed in Dataset EV2.

Generation of *brat* overexpression lines

brat coding sequence was recombined into the Gateway pDONR221 vector. Single nucleotide modifications were generated using QuikChange Lightning Site-directed Mutagenesis Kit (Agilent Technologies). The *brat* RNAi (TID 105054)-resistant sequence was generated using a custom-made Perl script, and the resulting fragment was *de novo* synthesized (Mr. Gene, Life Technologies). The newly synthesized fragment, covering the attL1 site of the pDONR221 vector and the *brat* RNAi-resistant part, was cloned into pDONR221-*brat* backbone using the enzymes ApaI and BbvCI. *brat* modified and unmodified coding sequences were recombined into the Gateway destination vector pUASt containing an N-terminal 3xFlag-6xMyc site and an attB site for landing site integration. Plasmids were injected into flies that contain an attP-landing site with PhiC31 activity at the third chromosome (MM2).

Generation of *V5::brat* and *zld-RB::V5* using the Cas9/CRISPR system

Endogenous *V5::brat* and *zld*::V5 were generated using the Cas9/CRISPR technology as described in [41]. Briefly, a donor oligo, which contains the V5 tag and about 60 nucleotides homologues to the *brat* or *zld* gene upstream and downstream of the V5-tag integration site, was synthesized by Integrated DNA Technology (http://eu.idtdna.com/site):

V5::brat:5′GCTGTTACTCCTAAAGGTAAACGGAGCCACCGACGGCACTTACAACAtAAAGATGGGTAAGCCTATACCTAACCCTCTTCTTGGTCTAGATAGCACGGCGAGTTCGCCGACACCATCTCTGGACTCGATGCGGGGCGGGGCGAACTCGATTGAATCATAC

zld::V5:5′ATCAAGAGCGAGTACGTGCAGGAGGAGTTTCAGATGATCGAGAAGAGCATAGAGCTCTACGGTAAGCCTATACCTAACCCTCTTCTTGGTCTAGATAGCACGTGAATGAGTGGGCAGGCCACTGGGTTCTGGGTTTTGAAATGCTCCTAGGCTTTGAGCTTGTCT

Guidance RNAs (*brat*: CACCGACACCATCTCTGGAC, *zld*: ATAGAGCTCTACTGAATGAG) were cloned into the CRISPR/Cas9 vector [41] and transfected together with the donor oligo into w^{1118} flies. Transgenic flies were screened by PCR flanking the V5-tag region.

Antibodies

Antibodies used in this study were guinea pig anti-Dpn, 1:1,000, [42]; rat anti-Ase, 1:500, [42]; chicken anti-GFP (Abcam); rabbit anti-Brat, 1:100, [9]; mouse anti-pH3 (Cell Signaling Technology); mouse anti-V5 (Sigma-Aldrich); mouse anti-Myc (9E10); mouse anti-Flag M2 (Sigma-Aldrich); mouse anti-Lamin ADL67.10 (DSHB); mouse anti-Bruchpilot nc82, 1:10 (DSHB); guinea pig anti-Mira, 1:250; rabbit anti-Hamlet, 1:50 (homemade, [42]); rabbit anti-Dichaete, 1:1,000, [64]; mouse anti-Eyeless, 1:10 (DSHB), rat anti-Grainy head, 1:1,000, [14].

Immunohistochemistry

For immunofluorescence, larval or adult brains were dissected in PBS, fixed for 20 min in 5% paraformaldehyde (PFA) in PBS (larvae) or in 5% PFA with 0.1% Triton X-100 (adult), and blocked in 1% normal goat serum (NGS) (larvae) or 5% NGS (adult) in PBS with 0.1% Triton X-100 (blocking solution), and antibodies were diluted in blocking solution. Brains were mounted in Vectashield (Vector Laboratories). Fluorescence *in situ* hybridization (FISH) protocol was adapted from [65] and Stellaris protocols. Larval brains were dissected in PBS, fixed for 20 min in 4% PFA in PBS/DEPC, and permeabilized in 70% EtOH for at least 24 h at 4°C. 250 nM final concentration of Stellaris probes in hybridization buffer was used and incubated overnight with larval brains in the dark at 37°C. Brains were mounted in 2× SSC and imaged the same day. Confocal images were acquired on LSM780 microscopes (Carl Zeiss GmbH).

Quantification of Brat, Myc::Brat, Zld-PB::V5, and Dpn expression

Quantification of protein expression was performed using the Histo feature of the ZEN software. Membrane-bound GFP was used to outline the respective cell section (at its biggest appearance), and the mean intensity of Brat, Myc::Brat, or Dpn levels were measured.

Brain tumor transplantation and metastasis quantification

L3 brains from UAS-dcr2/UAS-*brat* RNAi; wor-Gal4, ase-Gal80/+; UAS-Stinger::RFP/UAS-*mCherry* shmiR or UAS-dcr2/UAS-*brat* RNAi; wor-Gal4, ase-Gal80/UAS-*zld* shmiR; UAS-Stinger::RFP/+ were dissected and mechanically disrupted in PBS. RFP^+ cells concentration were estimated on a Neubauer cell counter, and ~500 cells were immediately intra-thoracically injected into 3- to 6-day-old adult females with a Nanoject II (Drummond). Bright-field, GFP and RFP pictures of living flies were taken on a Lumar fluorescence stereomicroscope/color SPOT camera repeatedly after transplantation. GFP autofluorescence signal was subtracted from tumor-specific RFP signal and displayed in false colors red-green-blue-cyan-magenta-yellow-white from least to most intense. Alternatively, the

RFP-specific signal was quantified on ImageJ from the raw intensity displayed in Measure tool on the delineated area of the whole fly. Intensities of all flies in one picture were averaged.

Cell dissociation, FACS, sample preparation, and RNA sequencing

Cell dissociation, FACS, and bioinformatic analysis were done as previously described with minor modifications [40,66]. UAS-dcr2; wor-Gal4, ase-Gal80; UAS-mCD8::GFP line was used to induce the expression of membrane-bound GFP and *brat* RNAi. GFP expression with and without *brat* RNAi was induced under the control of tub-Gal80^{ts} for 24 h. GFP-positive cells were sorted by FACS, and RNA of sorted cells was isolated. Seventy-six base pair Illumina paired-end sequencing of Poly-A-mRNA libraries was performed on GAIIx. The experiment lacked biological replicates due to difficulties in getting sufficient material to prepare the sequencing library. For the analysis, DESeq was instructed to ignore the condition labels and estimate the variance by treating all the samples as if they were replicates of the same condition (method = "blind") [67]. Sequencing results of selected hits were verified by qPCR. Around 200 larval brains were dissected to obtain sufficient GFP-positive cells per replicate of the qPCR experiment. First-strand cDNA was generated using random primers on TRIzol-extracted total FACS-sorted cell RNA. qPCR was done using Bio-Rad IQ SYBR Green Supermix on a Bio-Rad CFX96 cycler. Expression of each gene was normalized to RpS8, and relative levels were calculated using the $2^{-\Delta\Delta C_T}$ method [68]. Oligo sequences used for qPCR analysis of FACS-sorted samples are listed in Dataset EV2.

RNA immunoprecipitation (RIP)

RIP experiment was adopted from [69]. Briefly, 100 control and 50 *brat*^{K06028} mutant 3rd instar larval brains or 1 ml of control and Brat overexpression S2 cell culture were fixed in 0.5% formaldehyde. Fixed tissue was homogenized in RIP lysis buffer and briefly sonicated with a microtip sonicator. Brain samples were first incubated with 7.5 μg rabbit anti-Brat antibody and subsequently with Protein G dynabeads. S2 cell samples were incubated with 10 μl anti-Myc beads. Material elution and cross-linking reversal was performed by incubating samples in RIP elution. After RNA purification, pellets were resuspended in 20 μl H2O/DEPC and qPCR was performed. See Appendix Supplementary Methods and Dataset EV2.

Drosophila S2 cell reporter assay

dpn and *zld* 3′UTR including an N-terminal stop codon were cloned from *Drosophila* genomic DNA (oligos used for PCR, see Dataset EV2) and recombined first into the Gateway pDONR221 vector and subsequently into the Gateway destination vector pAGW containing an Actin5C promoter and a GFP coding sequence (The Drosophila Gateway vector collection). GFP control reporter: A SV40 terminator sequence was recombined into pAGW. *Drosophila* S2R$^+$ cells were cotransfected with GFP control/3′UTR reporter, Actin5C-RFP expression vector (transfection control) and Actin5C-lacZ/Brat overexpression vector. RFP transfected cells were preselected by FACSCanto II Flow Cytometer, and GFP intensity mean of RFP-positive cells was measured. Three independent transfections were analyzed. Mycoplasma contamination was not checked.

EMSA experiment

The approximately 150-nt-long fragments of the *zld* and *dp*n 3′UTR and point mutants thereof were *in vitro* transcribed from PCR-amplified DNA templates using oligos listed in Dataset EV2. *In vitro* transcription, protein purification and native gel electrophoresis were essentially carried out as described in [27]. Point mutations were introduced by site-directed mutagenesis [70] with oligos listed in Dataset EV2.

Statistics

Statistical analyses were performed with GraphPad Prism 7. Unpaired two-tailed Student's *t*-test was used to assess statistical significance between two genotypes/conditions. No statistical methods were used to predetermine the sample size. Sample sizes for experiments were estimated based on previous experience with a similar setup that showed significance. Experiments were not randomized, and investigator was not blinded. No samples or animals were excluded from our analysis.

Data availability

RNA sequencing data have been submitted to NCBI GEO project Accession Number GSE104592.

Expanded View for this article is available online.

Acknowledgements
We wish to thank Elke Kleiner, Peter Duchek, Sara Farina Lopez, Joseph Francis Gokcezade, and Merve Deniz Abdusellamoglu for technical assistance; all members of the J.A.K. laboratory for discussions; S.G. Tsitilou for sharing reagents; F.B. was supported by an EMBO Long-Term Fellowship (LTF 1280-2014). Work in the J.A.K. laboratory is supported by the Austrian Academy of Sciences, the EU Seventh Framework Programme network EuroSyStem, the Austrian Science Fund (grants I_552-B19 and Z_153_B09), and the advanced grants of the European Research Council 250342 (NeuroSyStem) and 695642 (MiniBrain).

Author contributions
IR, FB, and JAK designed and interpreted experiments. IR, FB, and VS performed the experiments. IL performed Brat–RNA interaction (EMSA) experiments. TRB performed RNA-seq data analysis. GM supervised the work of IL. IR and JAK wrote the manuscript with input from all authors.

Conflict of interest
The authors declare that they have no conflict of interest.

Reference

1. Caussinus E, Gonzalez C (2005) Induction of tumor growth by altered stem-cell asymmetric division in *Drosophila melanogaster*. *Nat Genet* 37: 1125 – 1129
2. Knoblich JA (2010) Asymmetric cell division: recent developments and their implications for tumour biology. *Nat Rev Mol Cell Biol* 11: 849 – 860
3. Inaba M, Yamashita YM (2012) Asymmetric stem cell division: precision for robustness. *Cell Stem Cell* 11: 461 – 469

4. Homem CCF, Knoblich JA (2012) *Drosophila* neuroblasts: a model for stem cell biology. *Development* 139: 4297 – 4310
5. Reichert H (2011) *Drosophila* neural stem cells: cell cycle control of self-renewal, differentiation, and termination in brain development. *Results Probl Cell Differ* 53: 529 – 546
6. Weng M, Lee C-Y (2011) Keeping neural progenitor cells on a short leash during *Drosophila* neurogenesis. *Curr Opin Neurobiol* 21: 36 – 42
7. Hirata J, Nakagoshi H, Nabeshima Y, Matsuzaki F (1995) Asymmetric segregation of the homeodomain protein Prospero during *Drosophila* development. *Nature* 377: 627 – 630
8. Knoblich JA, Jan LY, Jan YN (1995) Asymmetric segregation of Numb and Prospero during cell division. *Nature* 377: 624 – 627
9. Betschinger J, Mechtler K, Knoblich JA (2006) Asymmetric segregation of the tumor suppressor brat regulates self-renewal in *Drosophila* neural stem cells. *Cell* 124: 1241 – 1253
10. Guo M, Jan LY, Jan YN (1996) Control of daughter cell fates during asymmetric division: interaction of Numb and Notch. *Neuron* 17: 27 – 41
11. Choksi SP, Southall TD, Bossing T, Edoff K, de Wit E, Fischer BE, van Steensel B, Micklem G, Brand AH (2006) Prospero acts as a binary switch between self-renewal and differentiation in *Drosophila* neural stem cells. *Dev Cell* 11: 775 – 789
12. Couturier L, Mazouni K, Schweisguth F (2013) Numb localizes at endosomes and controls the endosomal sorting of notch after asymmetric division in *Drosophila*. *Curr Biol* 23: 588 – 593
13. Karcavich R, Doe CQ (2005) *Drosophila* neuroblast 7-3 cell lineage: a model system for studying programmed cell death, Notch/Numb signaling, and sequential specification of ganglion mother cell identity. *J Comp Neurol* 481: 240 – 251
14. Baumgardt M, Karlsson D, Terriente J, Díaz-Benjumea FJ, Thor S (2009) Neuronal subtype specification within a lineage by opposing temporal feed-forward loops. *Cell* 139: 969 – 982
15. Bello BC, Izergina N, Caussinus E, Reichert H (2008) Amplification of neural stem cell proliferation by intermediate progenitor cells in *Drosophila* brain development. *Neural Dev* 3: 5
16. Boone JQ, Doe CQ (2008) Identification of *Drosophila* type II neuroblast lineages containing transit amplifying ganglion mother cells. *Dev Neurobiol* 68: 1185 – 1195
17. Bowman SK, Rolland V, Betschinger J, Kinsey KA, Emery G, Knoblich JA (2008) The tumor suppressors Brat and Numb regulate transit-amplifying neuroblast lineages in *Drosophila*. *Dev Cell* 14: 535 – 546
18. Bier E, Vaessin H, Younger-Shepherd S, Jan LY, Jan YN (1992) deadpan, an essential pan-neural gene in *Drosophila*, encodes a helix-loop-helix protein similar to the hairy gene product. *Genes Dev* 6: 2137 – 2151
19. Lee C-Y, Wilkinson BD, Siegrist SE, Wharton RP, Doe CQ (2006) Brat is a Miranda cargo protein that promotes neuronal differentiation and inhibits neuroblast self-renewal. *Dev Cell* 10: 441 – 449
20. Song Y, Lu B (2011) Regulation of cell growth by Notch signaling and its differential requirement in normal vs. tumor-forming stem cells in *Drosophila*. *Genes Dev* 25: 2644 – 2658
21. Xiao Q, Komori H, Lee C-Y (2012) klumpfuss distinguishes stem cells from progenitor cells during asymmetric neuroblast division. *Development* 139: 2670 – 2680
22. Janssens DH, Komori H, Grbac D, Chen K, Koe CT, Wang H, Lee CY (2014) Earmuff restricts progenitor cell potential by attenuating the competence to respond to self-renewal factors. *Development* 141: 1036 – 1046
23. Arama E, Dickman D, Kimchie Z, Shearn A, Lev Z (2000) Mutations in the beta-propeller domain of the *Drosophila* brain tumor (brat) protein induce neoplasm in the larval brain. *Oncogene* 19: 3706 – 3716
24. Cho PF, Gamberi C, Cho-Park YA, Cho-Park IB, Lasko P, Sonenberg N (2006) Cap-dependent translational inhibition establishes two opposing morphogen gradients in *Drosophila* embryos. *Curr Biol* 16: 2035 – 2041
25. Sonoda J, Wharton RP (2001) *Drosophila* brain tumor is a translational repressor. *Genes Dev* 15: 762 – 773
26. Harris RE, Pargett M, Sutcliffe C, Umulis D, Ashe HL (2011) Brat promotes stem cell differentiation via control of a bistable switch that restricts BMP signaling. *Dev Cell* 20: 72 – 83
27. Loedige I, Stotz M, Qamar S, Kramer K, Hennig J, Schubert T, Loffler P, Langst G, Merkl R, Urlaub H *et al* (2014) The NHL domain of BRAT is an RNA-binding domain that directly contacts the hunchback mRNA for regulation. *Genes Dev* 28: 749 – 764
28. Laver JD, Li X, Ray D, Cook KB, Hahn NA, Nabeel-Shah S, Kekis M, Luo H, Marsolais AJ, Fung KY *et al* (2015) Brain tumor is a sequence-specific RNA-binding protein that directs maternal mRNA clearance during the *Drosophila* maternal-to-zygotic transition. *Genome Biol* 16: 94
29. Loedige I, Jakob L, Treiber T, Ray D, Stotz M, Treiber N, Hennig J, Cook KB, Morris Q, Hughes TR *et al* (2015) The crystal structure of the NHL domain in complex with RNA reveals the molecular basis of *Drosophila* brain-tumor-mediated gene regulation. *Cell Rep* 13: 1206 – 1220
30. Neumüller RA, Betschinger J, Fischer A, Mechtler K, Cohen SM, Knoblich JA (2008) Mei-P26 regulates microRNAs and cell growth in the *Drosophila* ovarian stem cell lineage. *Nature* 454: 241 – 245
31. Komori H, Xiao Q, McCartney BM, Lee C-Y (2013) Brain tumor specifies intermediate progenitor cell identity by attenuating β-catenin/Armadillo activity. *Development* 141: 51 – 62
32. Staudt N, Fellert S, Chung H-R, Jäckle H, Vorbrüggen G (2006) Mutations of the *Drosophila* zinc finger-encoding gene vielfältig impair mitotic cell divisions and cause improper chromosome segregation. *Mol Biol Cell* 17: 2356 – 2365
33. Liang H-L, Nien C-Y, Liu H-Y, Metzstein MM, Kirov N, Rushlow C (2008) The zinc-finger protein Zelda is a key activator of the early zygotic genome in *Drosophila*. *Nature* 456: 400 – 403
34. Harrison MM, Li X-Y, Kaplan T, Botchan MR, Eisen MB (2011) Zelda binding in the early *Drosophila melanogaster* embryo marks regions subsequently activated at the maternal-to-zygotic transition. *PLoS Genet* 7: e1002266
35. Nien C-Y, Liang H-L, Butcher S, Sun Y, Fu S, Gocha T, Kirov N, Manak JR, Rushlow C (2011) Temporal coordination of gene networks by Zelda in the early *Drosophila* embryo. *PLoS Genet* 7: e1002339
36. Giannios P, Tsitilou SG (2013) The embryonic transcription factor Zelda of *Drosophila melanogaster* is also expressed in larvae and may regulate developmentally important genes. *Biochem Biophys Res Comm* 438: 329 – 333
37. Suster ML, Seugnet L, Bate M, Sokolowski MB (2004) Refining GAL4-driven transgene expression in *Drosophila* with a GAL80 enhancer-trap. *Genesis* 39: 240 – 245
38. Pearson JC, Watson JD, Crews ST (2012) *Drosophila melanogaster* Zelda and single-minded collaborate to regulate an evolutionarily dynamic CNS midline cell enhancer. *Dev Biol* 366: 420 – 432
39. Hamm DC, Bondra ER, Harrison MM (2015) Transcriptional activation is a conserved feature of the early embryonic factor Zelda that requires a cluster of four zinc fingers for DNA binding and a low-complexity activation domain. *J Biol Chem* 290: 3508 – 3518

40. Berger C, Harzer H, Burkard TR, Steinmann J, van der Horst S, Laurenson A-S, Novatchkova M, Reichert H, Knoblich JA (2012) FACS purification and transcriptome analysis of *Drosophila* neural stem cells reveals a role for klumpfuss in self-renewal. *Cell Rep* 2: 407 – 418
41. Gokcezade J, Sienski G, Duchek P (2014) Efficient CRISPR/Cas9 plasmids for rapid and versatile genome editing in *Drosophila*. *G3 (Bethesda)* 4: 2279 – 2282
42. Eroglu E, Burkard TR, Jiang Y, Saini N, Homem CCF, Reichert H, Knoblich JA (2014) SWI/SNF complex prevents lineage reversion and induces temporal patterning in neural stem cells. *Cell* 156: 1259 – 1273
43. Homem CCF, Reichardt I, Berger C, Lendl T, Knoblich JA (2013) Long-term live cell imaging and automated 4D analysis of *Drosophila* neuroblast lineages. *PLoS One* 8: e79588
44. San-Juán BP, Baonza A (2011) The bHLH factor Deadpan is a direct target of Notch signaling and regulates neuroblast self-renewal in *Drosophila*. *Dev Biol* 352: 70 – 82
45. Zhu S, Wildonger J, Barshow S, Younger S, Huang Y, Lee T (2012) The bHLH repressor Deadpan regulates the self-renewal and specification of *Drosophila* larval neural stem cells independently of notch. *PLoS One* 7: e46724
46. San-Juán BP, Andrade-Zapata I, Baonza A (2012) The bHLH factors Dpn and members of the E(spl) complex mediate the function of Notch signalling regulating cell proliferation during wing disc development. *Biol Open* 1: 667 – 676
47. Cho PF, Poulin F, Cho-Park YA, Cho-Park IB, Chicoine JD, Lasko P, Sonenberg N (2005) A new paradigm for translational control: inhibition via 5′-3′ mRNA tethering by bicoid and the eIF4E cognate 4EHP. *Cell* 121: 411 – 423
48. Temme C, Zhang L, Kremmer E, Ihling C, Chartier A, Sinz A, Simonelig M, Wahle E (2010) Subunits of the *Drosophila* CCR4-NOT complex and their roles in mRNA deadenylation. *RNA* 16: 1356 – 1370
49. Smibert CA, Lie YS, Shillinglaw W, Henzel WJ, Macdonald PM (1999) Smaug, a novel and conserved protein, contributes to repression of nanos mRNA translation *in vitro*. *RNA* 5: 1535 – 1547
50. Dahanukar A, Walker JA, Wharton RP (1999) Smaug, a novel RNA-binding protein that operates a translational switch in *Drosophila*. *Mol Cell* 4: 209 – 218
51. Tadros W, Goldman AL, Babak T, Menzies F, Vardy L, Orr-Weaver T, Hughes TR, Westwood JT, Smibert CA, Lipshitz HD (2007) SMAUG is a major regulator of maternal mRNA destabilization in *Drosophila* and its translation is activated by the PAN GU kinase. *Dev Cell* 12: 143 – 155
52. Chen G, Kong J, Tucker-Burden C, Anand M, Rong Y, Rahman F, Moreno CS, Van Meir EG, Hadjipanayis CG, Brat DJ (2014) Human Brat ortholog TRIM3 is a tumor suppressor that regulates asymmetric cell division in glioblastoma. *Can Res* 74: 4536 – 4548
53. Worringer KA, Rand TA, Hayashi Y, Sami S, Takahashi K, Tanabe K, Narita M, Srivastava D, Yamanaka S (2014) The let-7/LIN-41 pathway regulates reprogramming to human induced pluripotent stem cells by controlling expression of prodifferentiation genes. *Cell Stem Cell* 14: 40 – 52
54. Hansen DV, Lui JH, Parker PRL, Kriegstein AR (2010) Neurogenic radial glia in the outer subventricular zone of human neocortex. *Nature* 464: 554 – 561
55. Lui JH, Hansen DV, Kriegstein AR (2011) Development and evolution of the human neocortex. *Cell* 146: 18 – 36
56. Ye B, Petritsch C, Clark IE, Gavis ER, Jan LY, Jan Y-N (2004) Nanos and Pumilio are essential for dendrite morphogenesis in *Drosophila* peripheral neurons. *Curr Biol* 14: 314 – 321
57. Neumüller RA, Richter C, Fischer A, Novatchkova M, Neumüller KG, Knoblich JA (2011) Genome-wide analysis of self-renewal in *Drosophila* neural stem cells by transgenic RNAi. *Cell Stem Cell* 8: 580 – 593
58. Pfeiffer BD, Jenett A, Hammonds AS, Ngo T-TB, Misra S, Murphy C, Scully A, Carlson JW, Wan KH, Laverty TR *et al* (2008) Tools for neuroanatomy and neurogenetics in *Drosophila*. *Proc Natl Acad Sci USA* 105: 9715 – 9720
59. Weng M, Golden KL, Lee C-Y (2010) dFezf/Earmuff maintains the restricted developmental potential of intermediate neural progenitors in *Drosophila*. *Dev Cell* 18: 126 – 135
60. Lee T, Luo L (1999) Mosaic analysis with a repressible cell marker for studies of gene function in neuronal morphogenesis. *Neuron* 22: 451 – 461
61. Vert J-P, Foveau N, Lajaunie C, Vandenbrouck Y (2006) An accurate and interpretable model for siRNA efficacy prediction. *BMC Bioinformatics* 7: 520
62. Brennecke J, Stark A, Russell RB, Cohen SM (2005) Principles of microRNA-target recognition. *PLoS Biol* 3: e85
63. Haley B, Foys B, Levine M (2010) Vectors and parameters that enhance the efficacy of RNAi-mediated gene disruption in transgenic *Drosophila*. *Proc Natl Acad Sci USA* 107: 11435 – 11440
64. Ma Y, Niemitz EL, Nambu PA, Shan X, Sackerson C, Fujioka M, Goto T, Nambu JR (1998) Gene regulatory functions of *Drosophila* Fish-hook, a high mobility group domain Sox protein. *Mech Dev* 73: 169 – 182
65. Raj A, van den Bogaard P, Rifkin SA, van Oudenaarden A, Tyagi S (2008) Imaging individual mRNA molecules using multiple singly labeled probes. *Nat Methods* 5: 877 – 879
66. Harzer H, Berger C, Conder R, Schmauss G, Knoblich JA (2013) FACS purification of *Drosophila* larval neuroblasts for next-generation sequencing. *Nat Protoc* 8: 1088 – 1099
67. Anders S, Huber W (2010) Differential expression analysis for sequence count data. *Genome Biol* 11: R106
68. Livak KJ, Schmittgen TD (2001) Analysis of relative gene expression data using real-time quantitative PCR and the 2(-Delta Delta C(T)) Method. *Methods* 25: 402 – 408
69. Gilbert C, Svejstrup JQ (2006) RNA immunoprecipitation for determining RNA-protein associations *in vivo*. *Curr Protoc Mol Biol* Chapter 27: Unit 27.4
70. Zheng L, Baumann U, Reymond J-L (2004) An efficient one-step site-directed and site-saturation mutagenesis protocol. *Nucleic Acids Res* 32: e115

